iScience

Article

miR-29cb2 promotes angiogenesis and osteogenesis by inhibiting HIF-3α in bone

Liping Ouyang, Yingxiao Sun, Dan Lv, ..., Jun Ma, Xuanyong Liu, Yun Liao

libra_ly@shsmu.edu.cn (Y.L.)
xyliu@mail.sic.ac.cn (X.L.)
majun@shtrhospital.com (J.M.)

Highlights

Impaired osteogenesis and angiogenesis caused by miR-29cb2 deletion

HIF-3α is a novel target for miR-29cb2

Attenuated miR-29cb2 in bone accompany with elevated miR-29cb2 in peripheral blood

Article

miR-29cb2 promotes angiogenesis and osteogenesis by inhibiting HIF-3α in bone

Liping Ouyang,[1,4,9] Yingxiao Sun,[1,9] Dan Lv,[1] Xiaochun Peng,[5] Xiaoming Liu,[3] Lei Ci,[6] Guoning Zhang,[3] Bo Yuan,[1] Ling Li,[1] Jian Fei,[6,7] Jun Ma,[4,*] Xuanyong Liu,[2,8,*] and Yun Liao[1,10,*]

SUMMARY

Coordination between osteogenesis and angiogenesis is required for bone homeostasis. Here, we show that miR-29cb2 is a bone-specific miRNA and plays critical roles on angiogenesis-osteogenesis coupling during bone remodeling. Mice with deletion of miR-29cb2 exhibit osteopenic phenotypes and osteoblast impairment, accompanied by pronounced decreases in specific H vessels. The decrease in bone miR-29cb2 was associated with pathological ovariectomy stimuli. Mechanistically, hypoxia-inducible factor (HIF)-3α, as a target for miR-29cb2, inhibits HIF-1α activity by competitively bonding with HIF-1β. Notably, miR-29cb2 in peripheral blood (PB) nearly is undetectable in sham and significantly increases in ovariectomy mice. Further evaluation from osteoporosis patients demonstrates similar signatures. ROC analysis shows miR-29cb2 in PB has higher sensitivity and specificity for diagnosing osteoporosis when compared with four clinical biomarkers. Collectively, these findings reveal that miR-29cb2 is essential for bone remodeling by inhibiting HIF-3α and elevated bone-specific miR-29cb2 in PB, which may be a promising biomarker for bone loss

INTRODUCTION

Bone remodeling and vessel angiogenesis are inseparable for maintaining homeostatic bone renewal (Maes et al., 2010; Ramasamy et al., 2016) and its dysfunction frequently leads to diseases, such as osteoporosis (Huang et al., 2018). A subtype of capillaries with high CD31 and Endomucin expression (CD31hiEMCNhi), termed type H vessels, has been identified in the metaphysis near the growth plate (Kusumbe et al., 2014). Evidence indicates that type H vessel network is coupled with osteogenesis via signals from endothelial cells (Peng et al., 2020; Ramasamy et al., 2014) or bone cells (Xu et al., 2018; Xie et al., 2014). Proangiogenic factors, such as SLIT3 was secreted by CD31hiEMCNhi endothelial cells, which both enhances bone fracture healing and counteracted bone loss through SLIT-ROBO pathway (Xu et al., 2018); in addition, preosteoclasts-derived PDGF-BB induces CD31hiEMCNhi (Xie et al., 2014) angiogenesis for osteogenesis during bone modeling and remodeling. However, the specialized regulation and underlying coupling factors that both regulate angiogenesis and osteogenesis remain poorly understood.

Though the biological functions of miRNAs are not fully understood, it is clear that some miRNAs are present in a tissue-specific or cell-specific manner (Kloosterman and Plasterk, 2006), and play a crucial role in regulating neovascularization and osteogenesis (Douthitt et al., 2011; Small et al., 2010; Krzeszinski et al., 2014; Wang et al., 2019). miR-497~195 clusters are highly expressed in H vessels, and promote H vessels and bone formation via maintaining HIF-1α stability and Notch activity (Yang et al., 2017). Unfortunately, the mechanism is unclear because of the complexity of miR-497–195 clusters. The miR-29 gene family comprises two clusters: miR-29ab1 and miR-29cb2 (Kriegel et al., 2012), and each member of miR-29 family exhibits highly diverse characteristics in the regulation of gene expression and tissue development (He et al., 2007; Liu et al., 2010). Our recent study demonstrated that mice lack of miR-29ab1 exhibited an increase in the number of subcutaneous capillaries and miR-29 family was involved in regulation of endothelial function (Liao et al., 2019), which is consistent with previous reports (Hiroki et al., 2010; Widlansky et al., 2018).

In this study, we further found the complex functions of miR-29cb2 are bone-specific. miR-29cb2 was highly enriched in normal bone and was required to maintain angiogenesis and bone remodeling in adult mice. The knockout of miR-29cb2 (miR-29cb2−/−) exhibited suppressed osteoblastic bone formation and

[1]Department of Pharmacy, Tongren Hospital, Shanghai Jiao Tong University School of Medicine, Shanghai 200336, China

[2]State Key Laboratory of High Performance Ceramics and Superfine Microstructure, Shanghai Institute of Ceramics, Chinese Academy of Sciences, Shanghai 200050, China

[3]Department of Orthopedics, Tongren Hospital, Shanghai Jiao Tong University School of Medicine, Shanghai 200336, China

[4]Hongqiao International Institute of Medicine, Shanghai Jiao Tong University School of Medicine, Shanghai 200336, China

[5]Department of Orthopaedics, The Sixth Affiliated People's Hospital, Shanghai Jiaotong University, Shanghai 200233, China

[6]Shanghai Engineering Research Center for Model Organisms, Shanghai Model Organisms Center, INC., Shanghai 201203, China

[7]School of Life Science and Technology, Tongji University, Shanghai 200092, China

[8]School of Chemistry and Materials Science, Hangzhou Institute for Advanced Study, University of Chinese Academy of Sciences, Hangzhou 310024, China

[9]These authors contributed equally

[10]Lead contact

*Correspondence:
libra_ly@shsmu.edu.cn (Y.L.),
xyliu@mail.sic.ac.cn (X.L.),
majun@shtrhospital.com (J.M.)

https://doi.org/10.1016/j.isci.2021.103604

reduced type H vessels numbers. With osteoporosis-related bone loss, ovariectomy (OVX) mice showed gradual decreases in miR-29cb2 level of bone samples. Transcriptomic analysis further identified hypoxia-inducible factor (HIF)-3α could inhibit HIF-1 action by competing for binding to HIF-1β subunit, as a miR-29cb2-controlled target (Duan, 2016; Yang et al., 2015). In fact, the HIF family is a potent regulator of bone homeostasis as well as angiogenesis under relatively hypoxic conditions (Johnson et al., 2015).

Notably, miR-29cb2 in peripheral blood (PB) were present with very low abundance in normal mice, but significantly increased correlating with pathological stimuli in OVX mice. Recent reports show that miRNAs are present in various body fluid including blood (Kodahl et al., 2014; Schwarzenbach et al., 2014), and altered miRNA expression and specific signatures of tissue miRNAs have been associated with the diagnosis and prognosis for diseases (Joshi et al., 2015). We further examined the miR-29cb2 expressions in bone and PB from osteopenia and osteoporosis patients, and found that elevated bone-specific miR-29cb2 in PB was associated with bone loss in osteoporosis patients. By receiver operating characteristic (ROC) curve analysis, compared with four classic biomarkers, miR-29cb2 revealed the higher sensitivity and specificity for diagnosing osteoporosis. In the present study, we reported an exciting discovery that bone-specific miR-29cb2 coupled angiogenesis with bone remodeling via HIF-3α pathway, and elevated miR-29cb2 in blood may be a non-invasive biomarker for early detection of bone loss in humans.

RESULTS

Mice with deletion of miR-29cb2 exhibit osteopenic phenotypes and osteoblast impairment

miR-29cb2$^{-/-}$ mice were born healthy at the expected Mendelian ratios, with no apparent gross abnormalities. However, histological and micro-CT analyses revealed an age-associated low bone mass in the long bones. Micro-CT imaging demonstrated that the femurs of juvenile (6-week-old) miR-29cb2$^{-/-}$ mice had a normal phenotype (Figure 1A). Furthermore, adult (16-week-old) miR-29cb2$^{-/-}$ mice exhibited an osteopenic phenotype (Figure 1B). Relative to wild-type (WT) control mice, trabecular of miR-29cb2$^{-/-}$ mice had a decrease in the bone volume fraction (BV/TV, Figure 1C) and trabecular bone mineral density (BMD, Figure 1D) with concomitant increases in the trabecular pattern factor (TPF, Figure 1E) at 16 weeks, although trabecular thickness (Tb. Th, Figure 1F) was slightly lower after knocking miR-29cb2. There was no significance in Tb. N, Tb. Sp, and cortical BMD (Figure S1). Hematoxylin and eosin (HE) staining also revealed that miR-29cb2$^{-/-}$ mice exhibited normal growth plate architecture; however, the femurs of miR-29cb2$^{-/-}$ mice contained less trabecular bone than those of WT control mice at 16 weeks (Figures 1G and 1H), indicating that miR-29cb2 affected bone osteogenesis but not bone dysplasia.

To understand the relative contributions of osteoblast and osteoclast functions to the osteopenia seen in miR-29cb2$^{-/-}$ mice, we next performed histomorphometric analysis of WT and miR-29cb2$^{-/-}$ mice to evaluate bone formation and resorption. HE-stained sections revealed a significant decrease in the number of cuboidal osteoblasts lining the trabeculae of 16-week-old miR-29cb2$^{-/-}$ mice compared with WT mice of the same age (Figure 1I). In addition, we observed low osteoblast activity in 16-week-old miR-29cb2$^{-/-}$ mice, evidenced by the significant reduction in the level of the osteoblast marker runt-related transcription factor 2 (RUNX-2) compared with that in WT mice (Figures 1J and 1K). Osterix, downstream gene of Runx-2, was also attenuated in miR-29cb2 knockout mice (Figures 1L and 1M). Silencing miR-29cb2 caused a decrease in bone resorption. TRAP-stained sections revealed suppression of osteoclasts in homozygous miR-29cb2$^{-/-}$ mice at 16 weeks (Figures 1N and 1O). These results indicated that the osteopenic phenotype of mice with miR-29cb2 deficiency was caused mainly by an osteoblast-driven response rather than osteoclast defects. We further performed a more extensive real-time PCR (RT-PCR) analysis of characteristic osteoblast marker (*Bmp-4*, *Alp*, and *Runx-2*) and osteoclast marker (*Trap*) genes and observed similar results (Figure S2).

miR-29cb2$^{-/-}$ mice show an age-associated decrease in type H vessels *in vivo*

Type H vessels are characterized by a CD31^{hi}EMCN^{hi} phenotype (Kusumbe et al., 2014). Postnatal CD31^{hi}EMCN^{hi} endothelium grows quickly during puberty, but its growth decreases gradually as adulthood approaches (Wang et al., 2017). To assess the exact functions of miR-29cb2 in regulating type H vessels under physiological conditions, we examined the positive CD31^{hi}EMCN^{hi} endothelium in the metaphysis of the femur in WT and miR-29cb2$^{-/-}$ mice. In WT mice, the number of type H vessels was very high at 6 weeks after birth (Figures 2A and 2B) but was generally decreased by 40% at 16 weeks of age (Figures 2C and 2D), consistent with a previous report (Kusumbe et al., 2014). The amounts of EMCN-positive (Figures 2E and 2F), CD31-positive (Figures 2G and 2H) and double-positive endothelium were slightly lower in the
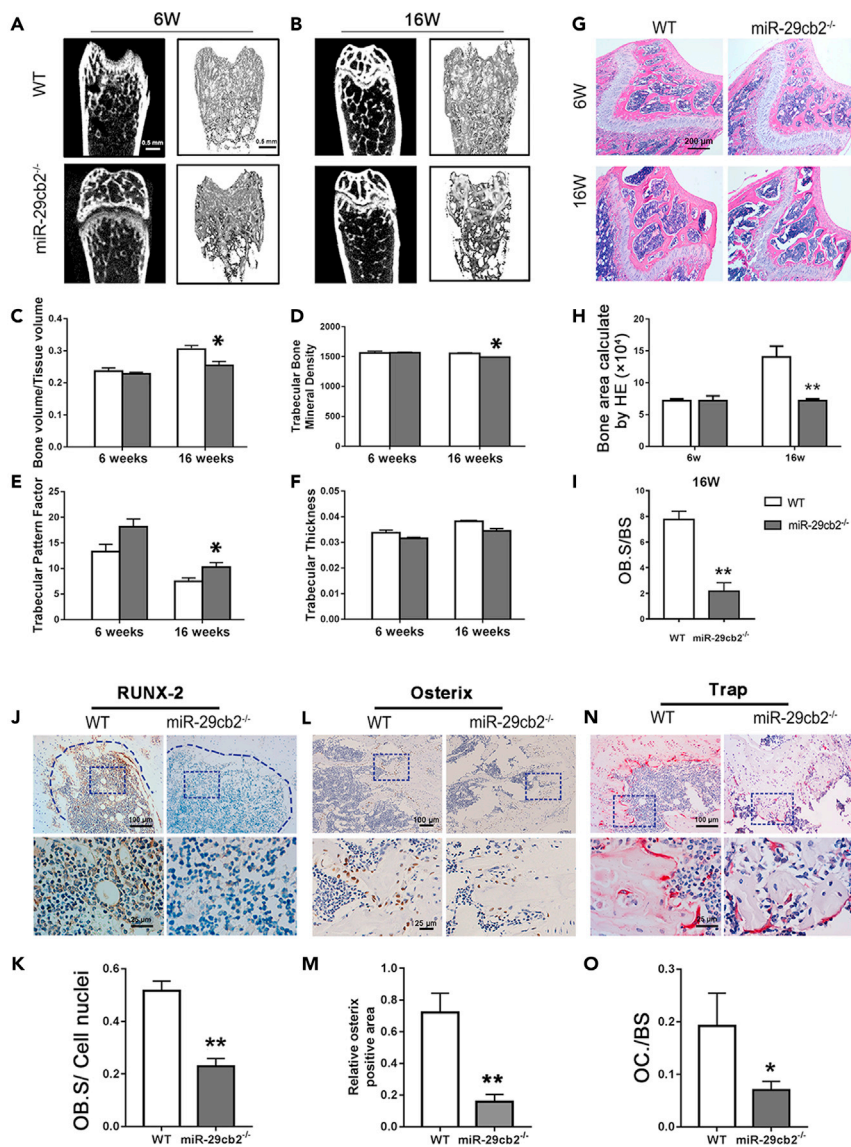
Figure 1. miR-29cb2 $^{-/-}$ mice show an osteopenic phenotype and osteoblast impairment

(A and B) Two-dimensionally and three-dimensionally reconstructed micro-CT images of WT, miR-29cb2$^{-/-}$ mice at 6. (A) and 16 (B) weeks of age. Scale bar: 0.5 mm.

(C–F) Bone-related parameters (bone volume/tissue volume, trabecular spacing, trabecular pattern factor, and trabecular thickness) of WT, miR-29cb2$^{-/-}$ at 6 and 16 weeks of age.

(G) HE staining of the femurs of WT and miR-29cb2$^{-/-}$ mice at 6 and 16 weeks of age (G). Scale bar: 200 μm.

(H and I) Trabecular bone content (H) and osteoblast/bone surface ratio (I) calculated from HE staining of 16-week-old mice bone.

(J and O) Representative immunostaining images and statistical data of RUNX-2 (J and K), Osterix (L and M), and Trap (N and O) expressions at 16 weeks. Scale bar: 100 μm and 25 μm. Values represent mean ± s.e.m. **p < 0.01 by one-way ANOVA followed by a Dunnett's test (C and E); **p < 0.01 by an unpaired two-tailed Student's t test (H, I, K, M, and O).

miR-29cb2$^{-/-}$ groups than in the WT group at 6 weeks, with a significant reduction at 16 weeks (Figures 2I– 2L). This result was consistent with the response of ossification to deletion of miR-29cb2 during bone remodeling stage. Considering these results collectively, we speculated that miR-29cb2 is a coupling factor that modulates both vessel angiogenesis and bone remodeling phenotypes. Impaired osteoblastic differentiation, possibly secondary to the reduction in type H vessels, thereby led to a decrease in bone formation in adult miR-29cb2$^{-/-}$ mice.
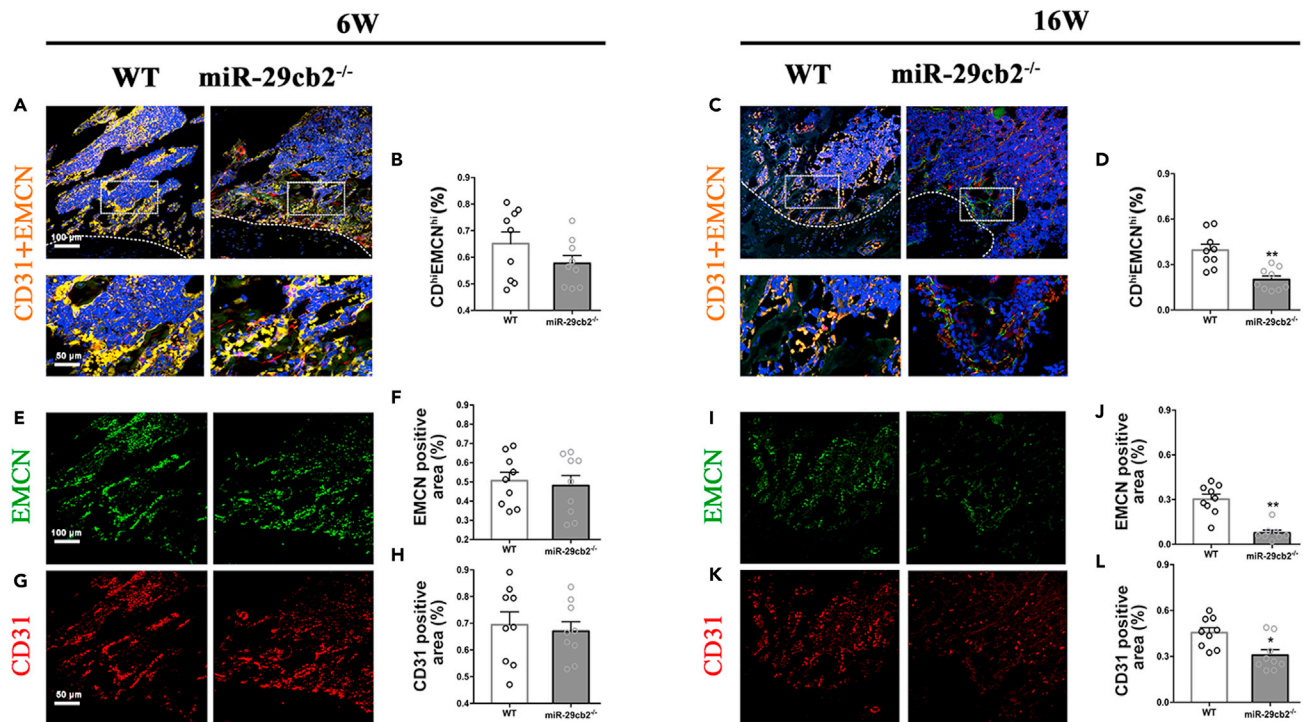
Figure 2. miR-29cb2$^{-/-}$ mice exhibit an age-associated decrease in CD31^{hi}EMCN^{hi} vessels

(A–D) Representative confocal images and statistical data of type H vessels in WT, miR-29cb2$^{-/-}$ mice at 6 (A and B) and 16 (C and D) weeks of age.

(E–H) Representative confocal images and statistical data of EMCN (E and F) and CD31 (G and H) labeled vessels in WT, miR-29cb2$^{-/-}$ mice at 6 weeks of age.

(I–L) Representative confocal images and statistical data of EMCN (I and J) and CD31 (K and L) labeled vessels in WT, miR-29cb2$^{-/-}$ mice at 16 weeks of age.

Scale bar: 100 and 50 μm. Values represent mean ± s.e.m. **$p < 0.01$ by one-way ANOVA followed by a Dunnett's test (B, D, F, H, J, and L)

Hif-3α mRNA is a new target of miR-29cb2

We next focused on identifying potential molecular mechanisms regulated by miR-29cb2 that signal for bone formation and vessel angiogenesis. To this end, we performed transcriptional profiling by RNA sequencing (RNA-seq) in 16-week-old WT and miR-29cb2$^{-/-}$ mice. A total of about 3800 genes exhibited altered expression after miR-29cb2 deletion in bone tissue (Figure 3A). Gene Ontology (GO) enrichment analysis demonstrated that the set of differentially expressed genes (DEGs) in miR-29cb2 versus WT trabecula was enriched with genes related to hypoxia (Figure 3B) in addition to the expected enrichment with genes related to bone formation (Figure S3) and angiogenesis (Figure S4). Venn diagrams were generated to show the overlapping gene sets of upregulated genes, predicted orthologs of target genes and genes responding to hypoxia in samples from miR-29cb2$^{-/-}$ mice compared with WT control mice. The results suggested that miR-29cb2 most likely targets *Hif-3α* mRNA, which promoted angiogenesis and osteogenesis (Figure 3C). Further investigation of some hypoxia-related genes also revealed that *Hif-3α* expression was substantially higher in miR-29cb2$^{-/-}$ mice (Figure 3D). HIF-3α is a dominant negative regulator that can inhibit the function of HIF-1α by competing for binding with the HIF-1β subunit. Computational analysis with TargetScan demonstrated that miR-29cb2 can target the sites comprising nucleotides 2250 to 2257 and 2352 to 2358, which are 8-mer and 7-mer-A1 target sites, respectively. This pattern extends to humans and other species (Figure 3E).

To confirm the hypothesis that miR-29cb2 binds to the 3′-UTR of *Hif-3α* mRNA, luciferase reporter vectors containing a WT *Hif-3α* 3′-UTR (WT-*Hif-3α*) or a mutated version of the *Hif-3α* 3′-UTR (MUT-*Hif-3α*) were constructed by sequentially mutating the predicted 14-bp miR-29cb2 binding site in the *Hif-3α* 3′-UTR. The WT-*Hif-3α* vector was cotransfected into HEK293 cells with either a miR-29cb2 lentiviral vector or scrambled control vector. The luciferase activity of WT- *Hif-3α* was significantly reduced in miR-29cb2-transfected cells compared with scrambled control-transfected cells. In contrast, this miR-29cb2-mediated repression of luciferase reporter activity was abolished in cells transfected with the MUT-*Hif-3α* vector (Figures 3F and 3G). We performed RT-PCR to assess the expression of *Hif* mRNA in miR-29cb2$^{-/-}$ mice. These

Figure 3. *Hif-3α* mRNA is a new target of miR-29cb2

(A) Hierarchical clustering based on 3794 variable genes by RNA-seq dataset in 16-week-old WT and miR-29cb2$^{−/−}$ mice (A, n = 3 mice per group).

(B) GO enrichment analysis of genes differentially expressed in two groups.
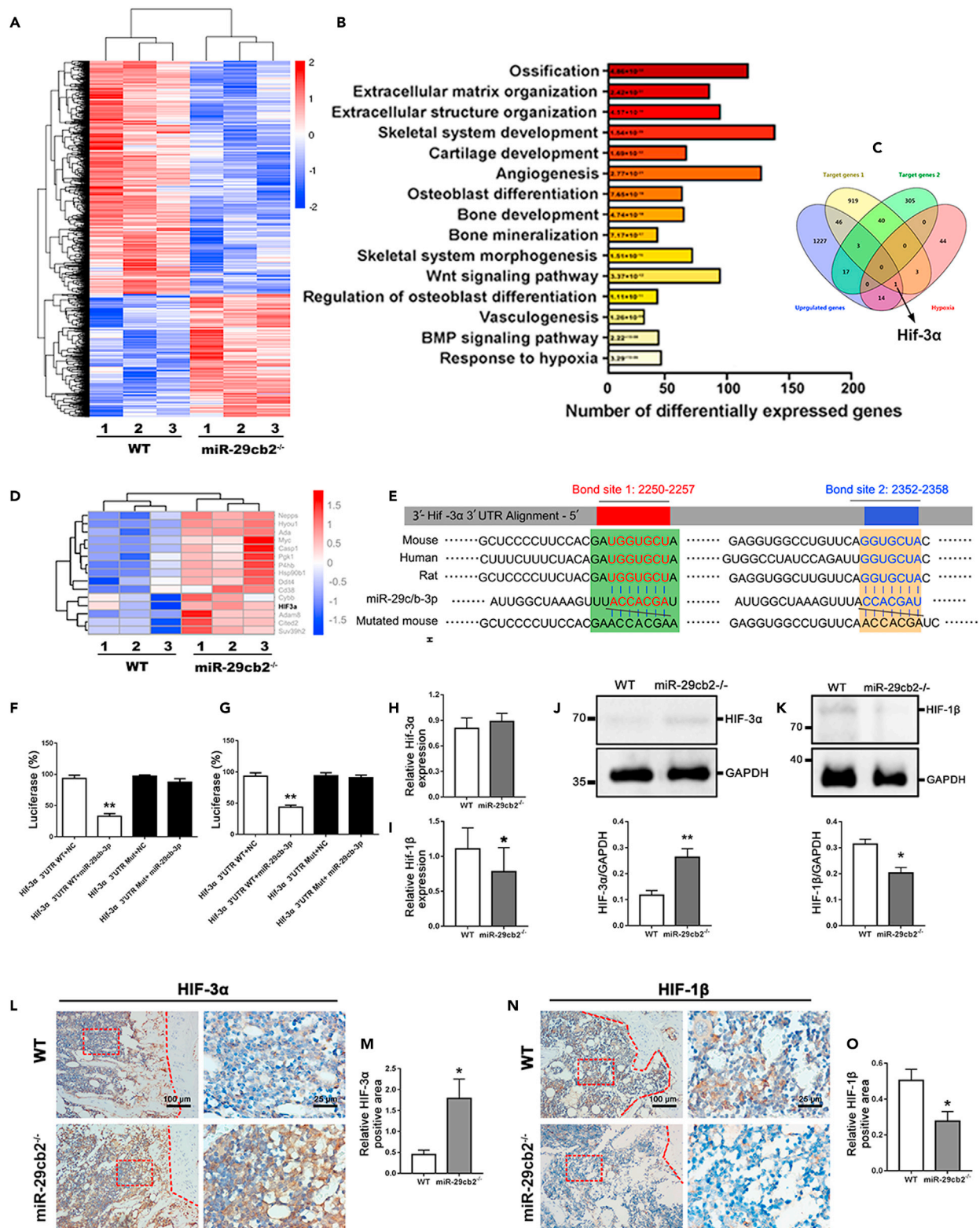
Figure 3. *Continued*

(C) Venn diagrams showing the overlapping gene sets of upregulated genes, predicted orthologs of target genes and genes responding to hypoxia in samples from miR-29cb2$^{-/-}$ mice compared with WT control mice.

(D) Heatmap of upregulated genes in the hypoxia pathway.

(E) Binding sites in *Hif-3α*.

(F and G) Luciferase activity of *Hif-3α* and bond site 1 (F) and site 2 (G) in the total cell lysates was assayed.

(H and I) Relative *Hif-3α* (H) and *Hif-1β* (I) mRNA expression in bone trabeculae from WT and miR-29cb2$^{-/-}$ mice.

(J and K) HIF-3α (J) and HIF-1β (K) protein levels in bone trabeculae from WT and miR-29cb2$^{-/-}$ mice by western blotting.

(L–O) Expression of HIF-3α (L and M) and HIF-1β (N and O) as assessed by immunostaining (brown). Scale bar: 100 and 25 μm. Values represent mean ± s.e.m. **p < 0.01 by one-way ANOVA followed by a Dunnett's test (F and G); **p < 0.01 by an unpaired two-tailed Student's *t* test (H–M, and O).

studies validated higher *Hif-3α* (Figure 3H) and substantially lower *Hif-1β* (Figure 3I) mRNA levels in the metaphyseal region in miR-29cb2$^{-/-}$ mice compared with WT mice at 16 weeks of age. Finally, nuclear accumulation assays (Figures 3J and 3K) and immunohistochemistry (Figures 3L–3O) revealed increased *Hif-3α* and decreased *Hif-1β* protein levels in bone samples from miR-29cb2$^{-/-}$ mice than those from WT mice.

To explore the molecular network encompassing miR-29cb2/HIF-3α in bone formation, we next focused on HIF-1α, a competitor of HIF-3α (Duan, 2016). In fact, HIF-1 is a potent regulator of bone homeostasis as well as angiogenesis (Kusumbe et al., 2014). When miR-29cb2 was silenced during bone remodeling the reduction in HIF-1 expression was accompanied by pronounced decreases in the expression of three crucial target genes: vascular endothelial growth factor (*Vegf*), *Runx-2*, and type II collagen 2a (*Col2a*) (Gilkes et al., 2014). These factors are representative of the central three steps in skeletal remodeling (vascularization, osteoblast differentiation, and collagen deposition (Figure S2).

miR-29cb2/HIF-3α pathway plays an essential role in OVX mice and osteoporosis patients

Our findings in genetically modified mice prompted us to further investigate the exact functions of miR-29cb2-regulated HIF-3α expression that connected bone formation with angiogenesis in response to pathological ovariectomy-related stimuli. The distal femurs from OVX mice showed a low bone mass associated with reduced trabecular parameters (Figure 4A), downregulated osteoblast activity (RUNX-2) (Figure S5), and reduced fluorescence from type H vessels (Figure 4B). Trabecular and cortical BMD both were not decreased in the OVX model (Figure S6). Adipose tissue area calculated from HE staining showed that more fat vacuoles can be observed in OVX mice femur than WT and miR-29cb2 knockout mice. Quantitative results showed that there were no significant differences between WT and miR-29cb2 knockout mice, whereas the adipose area of OVX mice was significantly higher than WT (Figure S7). Eight weeks after ovariectomy, the expressions of miR-29c/b2 in tissues are shown in Figures 4C–4E. The levels of miR-29cb2 in femur are markedly lower in OVX mice than in sham mice. In addition, miR-29c/b2 expressions of two typical adipose tissues collected from Sham and OVX mice, inguinal white adipose tissue (iWAT) and brown adipose tissue (BAT), were also evaluated and the results showed that miR-29c/b2 in iWAT and BAT did not exhibit any significance (Figure S8). Subsequently, we investigated whether down-regulation of miR-29cb2 in bone contributes to the up-regulation of HIF-3α. The protein levels of HIF-3α and HIF-1β were evaluated using western blotting and immunohistochemistry, and both approaches revealed a significant increase in HIF-3α (Figures 4F–4H) with a concomitant reduction in HIF-1β (Figures 4I–4K). The *Hif-3α* (Figure 4L) and *Hif-1β* (Figure 4M) mRNA levels showed similar patterns. These data were consistent with a report indicating that the increased amount of HIF-3α may be linked to impairment of angiogenesis followed by a delay in bone remodeling and suppression of osteoblast activity (Ando et al., 2013). The related mechanism of action is as follows: miR-29cb2 regulates osteogenesis and angiogenesis by targeting HIF-3α, which competitively binds to HIF-1β, resulting in a decrease in HIF-1α/β dimer formation (Figure 4N). This pathway has also been verified in bones of osteoporosis patients. Immunostaining and western blotting showed obviously higher HIF-3α and lower HIF-1β expression in the osteoporosis group than in the osteopenia group (Figures S9 and S10).

Elevated miR-29cb2 in peripheral blood (PB) is associated with bone loss

To characterize tissue-specific profiles of miR-29cb2 in osteoporosis, we analyzed the baseline and redistribution of the miR-29c/b2 in different organs between sham and OVX groups (Figures 4C and 4D). Under physiological conditions, the constitutive level of miR-29c/b2 was very high in normal bone, which was 30-fold to 600-fold higher in the femur than in tissues from the heart, liver, kidney, PB, and so on. After OVX for 8 weeks, the levels of miR-29c/b2 were significantly lower in the bone, whereas they were similar
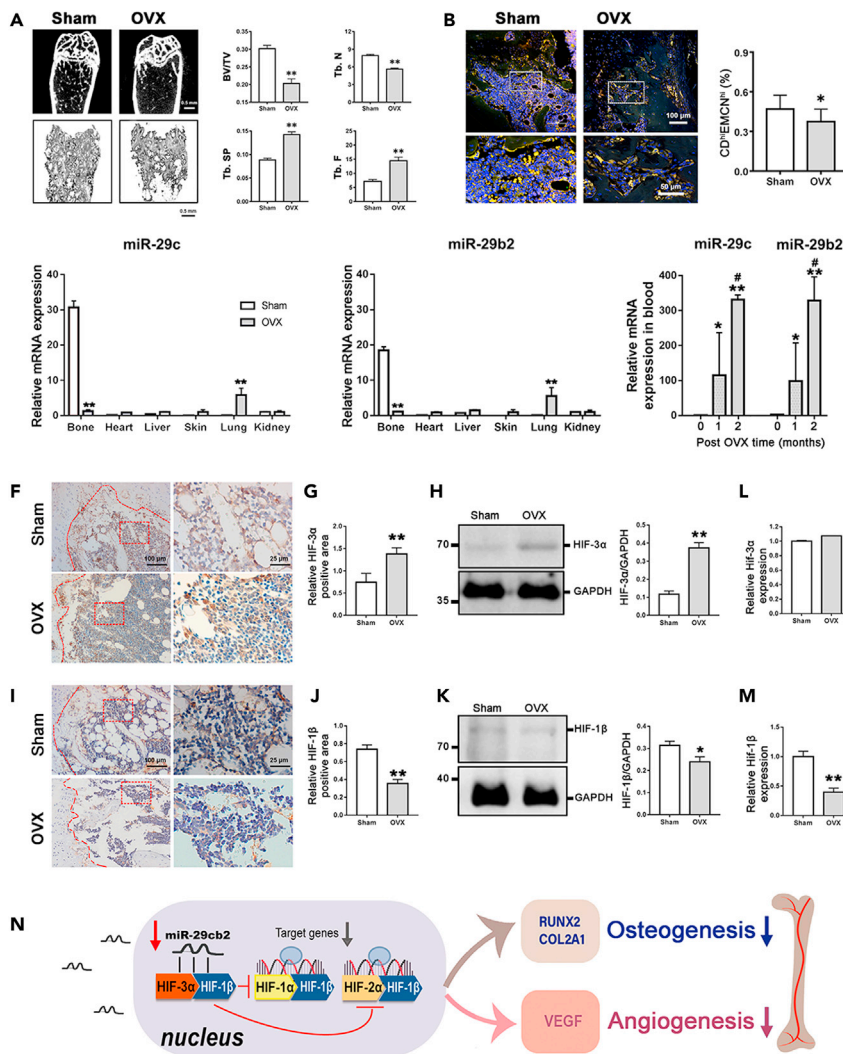
Figure 4. The miR-29cb2/HIF-3α pathway is present in OVX mice

(A) Two-dimensionally and three-dimensionally reconstructed micro-CT images and bone parameters (A). Scale bar: 0.5 mm.

(B) Representative confocal images and statistical data of H vessels in sham and OVX mice (B). Scale bar: 100 and 50 μm.

(C and D) Distribution of miR-29c (C) and miR-29b2 (D) in various organs and tissues.

(E) miR-29c and miR-29b2 expression in the blood of mice post OVX.

(F–H) HIF-3α expression assessed by immunostaining (F and G) and western blotting (H); Scale bar: 100 and 25 μm.

(I–K) HIF-1β expression assessed by immunostaining (I and J) and western blotting (K). Scale bar: 100 and 25 μm

(L and M) *Hif-3α* mRNA levels (L) and *Hif-1β* mRNA levels (M) in bone trabeculae assessed by RT-PCR in Sham and OVX mice.

(N) Mechanism by which miR-29cb2 promotes angiogenesis and osteogenesis via targeting of *Hif-3α* and preventing its competitive binding to *Hif-1β* (N). Values represent mean ± s.e.m. **p < 0.01 by an unpaired two-tailed Student's *t* test (A–D, F–H, and J–L) or by one-way ANOVA followed by a Dunnett's test (G and H); miR-29cb2 therapy for OVX mice.

in the liver, heart, and kidney between the two groups. In contrast, the levels of miR-29c/b2 in PB and lung were significantly higher in OVX mice than in sham mice, and the fold change in PB was the greatest among all tissues. Furthermore, we examined the miR-29c/b2 accumulation in the PB between 0, 4, and 8 weeks post-OVX, which gradually increased with osteoporosis development (Figure 4E). These results suggest that miR-29cb2 releasing from bone during osteoporosis are selectively and efficiently transferred to the PB, which gives the hint that miR-29cb2 could be a biomarker to osteoporosis.

To study the sensitive and specificity of miR-29cb2 to osteoporosis, we further explored the relationships of miR-29cb2 and osteoporosis in human subjects. Distal femur samples were collected from osteopenia and
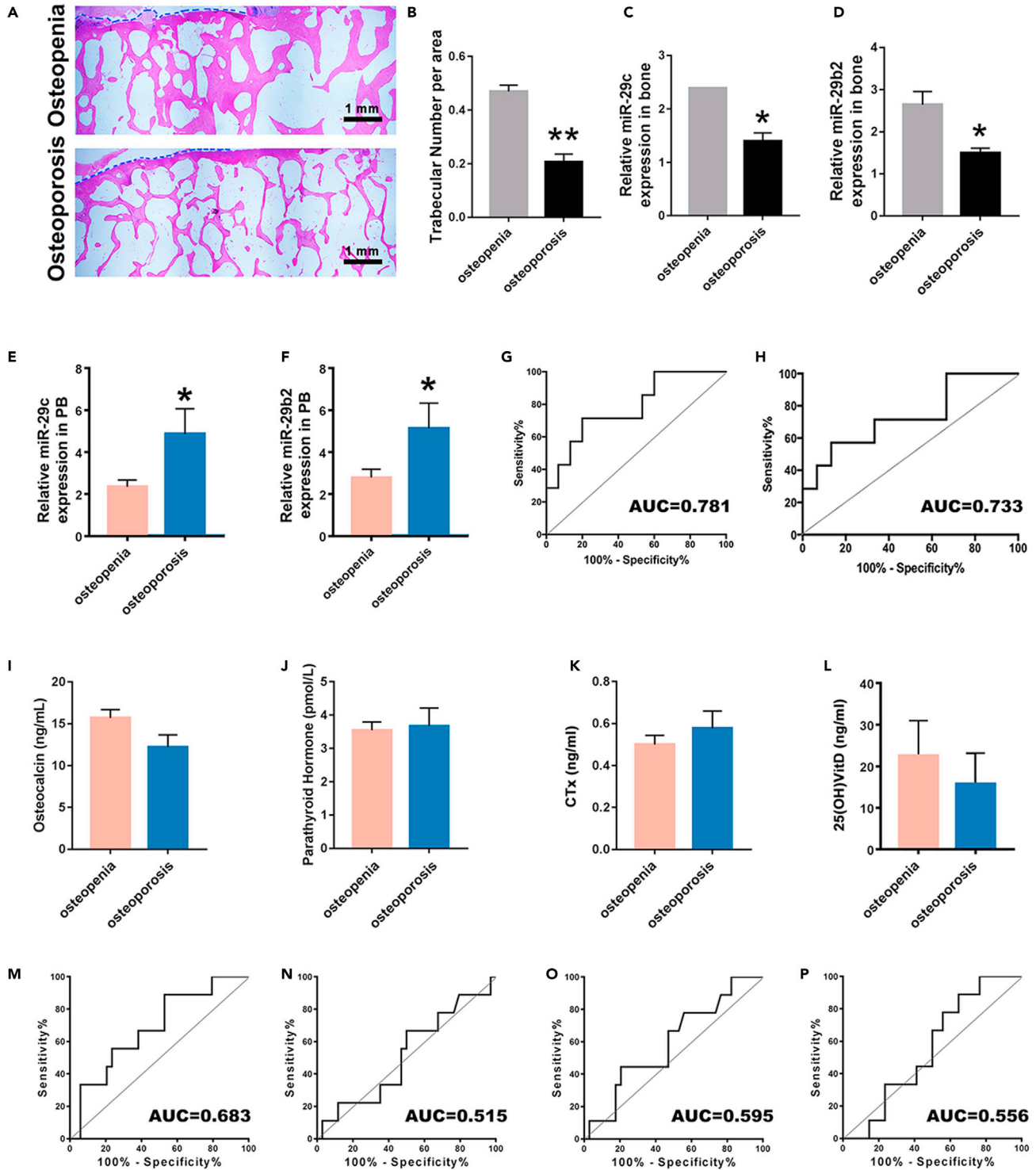
Figure 5. Elevation peripheral blood (PB) miR-29cb2 for diagnosing osteoporosis in patients

(A and B) HE staining of distal femur samples from osteopenia and osteoporosis patients (A) and the trabecular number per area calculated from the HE staining images (B). Scale bar: 1 mm.

(C and D) miR-29c (C) and miR-29b2 (D) expressions in distal femur of osteopenia and osteoporosis patients.

Figure 5. Continued

(E and F) miR-29c (E) and miR-29b2 level (F) in PB from the osteopenia and osteoporosis patients.

(G and H) ROC curve for evaluation of miR-29c and miR-29b2 as biomarkers to detect osteoporosis (G) and (H).

(I–P) Osteocalcin (I), parathyroid hormone (PTH) (J), collagen I degradation products (K), and 1,25(OH)$_2$VitD$_3$ (L) content and their ROC curve (M–P). Values represent mean $\pm$ s.e.m. **p < 0.01 by an unpaired two-tailed Student's t test (B–D).

osteoporosis patients for further study. HE staining showed obviously thinner trabecular bone (Figure 5A) and lower trabecular number per area in the osteoporosis group than in the osteopenia group (Figure 5B), which associated with a lower miR-29c/b2 expressions than osteopenia patients (Figures 5C and 5D). Then, we analyzed PB samples from 15 osteopenia patients (-1 >T-score > -2.5) and 7 osteoporosis patients (T-score < -2.5) in a cohort of subjects with similar ages (Figure S11). In these samples, the relative expressions of miR-29c/b2 were significantly higher in PB collected from osteoporosis patients than those from osteopenia patients (Figures 5E and 5F). The results in this small clinical cohort were consistent with OVX model, suggesting that elevated miR-29cb2 level in PB was correlated with the bone loss. Furthermore, ROC curve analysis was employed to estimate the diagnostic value of miR-29cb2. The area under the curve (AUC) value of miR-29c was 0.781 (95% confidence interval: 0.571 to 0.990) and was obtained (p < 0.05, Figure 5G) with comparable diagnostic sensitivity and specificity (Table S1). The AUC of miR-29b2 (95% CI: 0.496 to 0.970) was 0.733 (p = 0.08, Figure 5H and Table S2). We then performed a more extensive comparison of classic osteoporotic biomarker with miR-29cb2, including osteocalcin, parathyroid hormone (PTH), collagen I degradation products (CTx), and 25OHVitD. Our results showed that they were not significant difference between osteopenia and osteoporosis patients (Figures 5I–5L). The AUC of osteocalcin, parathyroid hormone (PTH), collagen I degradation products, and 25OHVitD in PB is 0.683, 0.515, 0.595, and 0.556, respectively (Figures 5M–5P). Compared to clinical serum marker, miR-29c is more sensitive and specific.

DISCUSSIONS

Bone is a highly vascularized organ. During bone modeling and remodeling, bone formation and vessel angiogenesis are inseparable and coupled (Peng et al., 2020; Sun et al., 2020). CD31^{hi}EMCN^{hi} or type H vessels have proven to be a specific endothelial feature identified in the murine skeletal system and exhibit potent osteogenic function (Wang et al., 2017). In turn, factors released from bone cells also affect type H vessel formation (Xie et al., 2014). The miR-29 family includes two clusters and plays complex functions in vessel and bone formation (Chen et al., 2017; Pan et al., 2016). In previous work, we found that miR-29ab1$^{-/-}$ mice (7-week-old) exhibited a phenotype of enhanced angiogenesis in subcutaneous tissue (Liao et al., 2019). In this study, we generated miR-29cb2$^{-/-}$ mice and found that the regulation of miR-29cb2 was essential in maintaining the properties of the CD31^{hi}EMCN^{hi} endothelium and bone homeostasis. miR-29cb2$^{-/-}$ mice exhibited a significant decrease in type H vessels, which contributed to the osteopenic phenotype observed in adult miR-29cb2$^{-/-}$ mice. This phenotype was not observed in juvenile miR-29cb2$^{-/-}$ mice, indicating that miR-29cb2 may influence mainly late bone remodeling, not early modeling. Generally, bone formation takes place independent of bone resorption during bone modeling, whereas bone resorption and formation occur simultaneously during bone remodeling to maintain skeletal homeostasis (Zaidi, 2007; Kenkre and Bassett, 2018). Our data provided several lines of evidence showing that miR-29cb2 participates in both osteoblast and osteoclast. Specific deletion of miR-29cb2 led to a significantly decreased osteoblast number and characteristic RUNX-2 and Osterix protein expression in the trabeculae of adult mice. Runx-2 is needed in processing multipotential mesenchymal progenitors differentiating to pre-osteoblasts (Jones et al., 2006). Pre-osteoblast differentiating to functional osteoblast requires Osterix (Nakashima et al., 2002). Knockout of miR-29cb2 attenuated both Runx-2 and Osterix expression, which leads to an impaired osteogenesis in miR-29cb2 knockout mice femur. Functional osteoblast biomarkers, *Bmp-4*, *Alp*, and *Runx-2* were reduced due to the decreased Runx-2 and Osterix expression. Trap staining verified that osteoclast function was impaired in miR-29cb2$^{-/-}$ mice. Similar to our findings, those of Zeng et al. indicated that miR-29b can promote osteoblast differentiation by modulating bone extracellular matrix proteins (Zeng et al., 2019). Collectively, these results indicate that suppressed osteoblastic bone formation contributes greatly to osteopenia in the context of miR-29cb2 deletion, which may provide new insight into the roles of miR-29cb2 in regulating distinct bone cells.

Complex pathogenic factors, including postmenopausal hormonal variation, drug, cancer, diabetes, and so on, are supposed to induce dysfunction of bone remodeling, which lead to osteopenia at the extensive stimuli (Chotiyarnwong and Mccloskey, 2020; Vanderwalde and Hurria, 2011). As reported in the references, animal models with single factor, such as OVX induced hormone decrease, show inferior effects on BMD than trabecular tissue volume. However, attenuated BMD and trabecular tissue volume usually

occur in the OVX model combined with other factors, such as glucocorticoid and methylprednisolone (Augat et al., 2003), which is consistent with our work (Figure S12 and Table S3). In fact, our data identified that the roles of miR-29cb2 were not only restricted in ovariectomized elicited osteopenia, but also in other diseases induced osteoporosis. A diabetes model showed an obvious decrease of miR-29c/b2 associated with reduced bone volume to the pathological stimuli (Figure S13). However, it is worthy to explore the role of miR-29cb2 in bone using more disease models and more observation time.

The balance of adipose and osteoblast is the most concerning issue in bone metabolism. miRNAs are identified to serve as the regulator of osteoblast and adipocyte differentiation to affect bone remodeling. Over expressions of miR-188 and miR-637 are verified to increase adipose accumulation and attenuate bone remodeling (Zhang et al., 2011; Li et al., 2015). miR-29 family participates in the metabolism of adipose depending on different subtypes. miR-29a supplement alleviates adipose formation through stabilizing RUNX-2 acetylation and restoring β-catenin levels via suppression of histone deacetylase 4 (HDAC4) (Ko et al., 2015), althoughmiR-29c has little effects on glucose related adipose regulation (Dooley et al., 2016). Our data showed that miR-29c deletion induced bone mass loss may be not attributed to adipose differentiation. References identify that miR-29c induced bone loss results from the dysfunction of osteoblast and osteoclast differentiation (Horita et al., 2021), which is consistent with our work.

Limited information is available about the miR-29cb2-regulated mechanisms that cause alterations in type H vessels and bone mass. Our data demonstrated that miR-29cb2 might regulate type H vessel formation and osteoblast function by targeting HIF-3α, which competitively inhibits HIF-1α activity. Bone is a relatively hypoxic tissue, and the oxygen tension (1%–7%) in bone is much lower than that in other adult tissues (20%). The function of HIF family is critical for maintaining bone remodeling (Johnson et al., 2015). HIF heterodimers comprise one of three α-subunits (HIF-1α, HIF-2α, or HIF-3α) and one β-subunit (Gonzalez et al., 2018; Kaelin and Ratcliffe, 2008). Studies showed that EC-specific deficiency of HIF-1α significantly reduces type H vessel formation and the function of nearby osteoblasts, leading to decreased bone formation (Kusumbe et al., 2014); moreover, knockout of HIF-2α in mice was shown to affect embryonic osteogenic differentiation and endochondral ossification, resulting in delayed cartilage development (Saito et al., 2010). Much less is known about HIF-3α than about HIF-1α and HIF-2α. The widely accepted belief is that HIF-3α is the inhibitory PAS domain protein (IPAS), which negatively affects gene expression by competing with HIF-1α or HIF-2α for binding to transcriptional elements (HIF-1β) in target genes (Ando et al., 2013; Zhang et al., 2014; Maynard et al., 2005). Consistent with the known role of HIF-3α, we observed that increased HIF-3α expression and reduced HIF-1β expression, associated with downregulated levels of HIF-1-mediated target genes (*Vegf*, C*ol-2a*, and *Runx-2*), then led to decreased angiogenesis coupled with repressed osteoblastic bone formation in the femurs of OVX and miR-29cb2$^{-/-}$ mice. We sought to highlight that miR-29cb2 regulates the expression of HIFs in a hypoxia-independent manner. Intracellular oxygen tension is not the only upstream regulator of HIF-3α (Zhang et al., 2014). The effects of miR-29cb2 deletion during bone development may differ between acute ischemic or hypoxic conditions, and the HIF-1 pathway was suppressed following overexpression of HIF-3α, likely explaining the osteoblast impairment and osteopenia observed in miR-29cb2$^{-/-}$ mice.

Different tissues display different characteristics of hypoxic responses, including changes in miRNA expressions that might result from tissue-specific (Ma et al., 2020; Corsten et al., 2010; Chen et al., 2019; Noren Hooten et al., 2010). In this study, RT-PCR analysis showed that the basal level of miR-29cb2 was much higher in bone than that in other organs under physiological bone homeostasis. With osteoporosis-related bone loss, the decrease in bone miR-29cb2 was associated with an inverse increase in PB miR-29cb2. This finding was consistent with reports indicating that miR-208a and miR-499-5p are highly enriched in heart tissue and considerable quantities of these miRNAs are rapidly released into PB following cardiac injury (Cheng et al., 2019). We thus speculate that miR-29cb2 is a bone-specific miRNA, and redistribution from bone to vessel could represent an angiogenesis-osteogenesis dysfunction. Typical clinical biomarkers of osteoporosis or osteopenia can be divided into four types: bone formation related biomarkers, bone resorption biomarkers, hormones, and nutrients related biomarkers (Ikebuchi et al., 2018; Xuan et al., 2015; Garnero, 2014; Boucher-Berry et al., 2012). In this study, four types of biomarkers, including osteocalcin, CTx, PTH, and 25OHVitD were tested. Unfortunately, their sensitivity and specificity for monitoring bone loss were lower than miR-29c/b2. It is worthy to further study the miR-29cb2 as bone loss biomarkers for monitoring osteoporosis.

In summary, these observations are compelling, as miR-29cb2 is a coupling factor and plays an essential permissive role during bone remodeling by downregulating the angiogenesis-osteogenesis

"brake" (i.e., HIF-3α) that keeps endothelial cells and osteoblasts in an angiogenic or osteogenic state; miR-29cb2 also is a bone-specific biomarker and selectively imported from bone to peripheral blood during angiogenesis-osteogenesis dysfunction. However, the means by which miR-29cb2 is transported into the circulation and the biological significance of this transport remain largely unknown.

Limitations of the study

Our data-driven analysis identifies that miR-29cb2 exhibits an essential role in bone remodeling, and has the potential to be a new biomarker for osteopenia. However, more disease models, longer observation time, and more patients should be studied for verifying the role of miR-29cb2 in osteopenia.

STAR★METHODS

Detailed methods are provided in the online version of this paper and include the following:

- KEY RESOURCES TABLE
- RESOURCE AVAILABILITY
  - Lead contact
  - Materials availability
  - Data and code availability
- EXPERIMENTAL MODEL AND SUBJECT DETAILS
- METHOD DETAILS
  - Labeling of CD31^{hi}EMCN^{hi} vessels
- BONE ANALYSIS
  - Micro-CT evaluation
  - Histopathological evaluation
  - RNA-seq and analysis
  - Luciferase activity
  - Quantitative RT-PCR (qRT-PCR)
  - Western blotting analysis
- HUMAN SAMPLE COLLECTION AND ASSESSMENT
  - Human distal femur evaluation
  - Peripheral blood (PB) collection and miR-29cb2 detection
  - Biomarkers evaluation
- QUANTIFICATION AND STATISTICAL ANALYSIS

SUPPLEMENTAL INFORMATION

Supplemental information can be found online at https://doi.org/10.1016/j.isci.2021.103604.

AUTHOR CONTRIBUTIONS

Y.X.S.: conducted experiments. L.P.O.Y., Y.X.S.: collection and/or assembly of data analysis, and interpretation. L.P.O.Y., Y.X.S. and Y. L.: manuscript writing. D.L., X.C.P., X.M.L., L.C., G.N.Z., B.Y., L.L., J.F.: provision of study materials. J.M., X.Y.L. and Y.L.: Financial support, final approval of manuscript.

DECLARATION OF INTERESTS

All authors declare that there are no conflicts of interest.

REFERENCES

Ando, H., Natsume, A., Iwami, K., Ohka, F., Kuchimaru, T., Kizaka-Kondoh, S., Ito, K., Saito, K., Sugita, S., Hoshino, T., et al. (2013). A hypoxia-inducible factor (HIF)-3α splicing variant, HIF-3α4 impairs angiogenesis in hypervascular malignant meningiomas with epigenetically silenced HIF-3α4. Biochem. Biophys. Res. Commun. 433, 139–144. https://doi.org/10.1016/j.bbrc.2013.02.044.

Augat, P., Schorlemmer, S., Gohl, C., Iwabu, S., Ignatius, A., and Claes, L. (2003). Glucocorticoid-treated sheep as a model for osteopenic trabecular bone in biomaterials research. J. Biomed. Mater. Res. A 66, 457–462. https://doi.org/10.1002/jbm.a.10601.

Boucher-Berry, C., Speiser, P.W., Carey, D.E., Shelov, S.P., Accacha, S., Fennoy, I., Rapaport, R., Espinal, Y., and Rosenbaum, M. (2012). Vitamin D, osteocalcin, and risk for adiposity as comorbidities in middle school children. J. Bone Miner Res. 27, 283–293. https://doi.org/10.1002/jbmr.550.

Camacho, P.M., Petak, S.M., Binkley, N., Diab, D.L., Eldeiry, L.S., Farooki, A., Harris, S.T., Hurley, D.L., Kelly, J., Lewiecki, E.M., et al. (2020). American association of clinical endocrinologists/American college of endocrinology clinical practice guidelines for the diagnosis and treatment of postmenopausal osteoporosis-2020 update. Endocr. Pract. 26, 1–46. https://doi.org/10.4158/GL-2020-0524.

Chen, L., Okeke, E., Ayalew, D., Wang, D., Shahid, L., and Dokun, A.O. (2017). Modulation of miR29a improves impaired post-ischemic angiogenesis in hyperglycemia. Exp. Biol. Med. (Maywood) 242, 1432–1443. https://doi.org/10.1177/1535370217716424.

Chen, Z., Bemben, M.G., and Bemben, D.A. (2019). Bone and muscle specific circulating microRNAs in postmenopausal women based on osteoporosis and sarcopenia status. Bone 120, 271–278. https://doi.org/10.1016/j.bone.2018.11.001.

Cheng, M., Yang, J., Zhao, X., Zhang, E., Zeng, Q., Yu, Y., Yang, L., Wu, B., Yi, G., Mao, X., et al. (2019). Circulating myocardial microRNAs from infarcted hearts are carried in exosomes and mobilise bone marrow progenitor cells. Nat. Commun. 10, 959. https://doi.org/10.1038/s41467-019-08895-7.

Chotiyarnwong, P., and Mccloskey, E.V. (2020). Pathogenesis of glucocorticoid-induced osteoporosis and options for treatment. Nat. Rev. Endocrinol. 16, 437–447. https://doi.org/10.1038/s41574-020-0341-0.

Corsten, M.F., Dennert, R., Jochems, S., Kuznetsova, T., Devaux, Y., Hofstra, L., Wagner, D.R., Staessen, J.A., Heymans, S., and Schroen, B. (2010). Circulating MicroRNA-208b and MicroRNA-499 reflect myocardial damage in cardiovascular disease. Circ. Cardiovasc. Genet. 3, 499–506. https://doi.org/10.1161/circgenetics.110.957415.

Dooley, J., Garcia-Perez, J.E., Sreenivasan, J., Schlenner, S.M., Vangoitsenhoven, R., Papadopoulou, A.S., Tian, L., Schonefeldt, S., Serneels, L., Deroose, C., et al. (2016). The microRNA-29 family dictates the balance between homeostatic and pathological glucose handling in diabetes and obesity. Diabetes 65, 53–61. https://doi.org/10.2337/db15-0770.

Douthitt, H.L., Luo, F., Mccann, S.D., and Meriney, S.D. (2011). Dynasore, an inhibitor of dynamin, increases the probability of transmitter release. Neuroscience 172, 187–195. https://doi.org/10.1016/j.neuroscience.2010.10.002.

Duan, C. (2016). Hypoxia-inducible factor 3 biology: complexities and emerging themes. Am. J. Physiol. Cell Physiol. 310, C260–C269. https://doi.org/10.1152/ajpcell.00315.2015.

Garnero, P. (2014). New developments in biological markers of bone metabolism in osteoporosis. Bone 66, 46–55. https://doi.org/10.1016/j.bone.2014.05.016.

Gilkes, D.M., Semenza, G.L., and Wirtz, D. (2014). Hypoxia and the extracellular matrix: drivers of tumour metastasis. Nat. Rev. Cancer 14, 430–439. https://doi.org/10.1038/nrc3726.

Gonzalez, F.J., Xie, C., and Jiang, C. (2018). The role of hypoxia-inducible factors in metabolic diseases. Nat. Rev. Endocrinol. 15, 21–32. https://doi.org/10.1038/s41574-018-0096-z.

He, A., Zhu, L., Gupta, N., Chang, Y., and Fang, F. (2007). Overexpression of micro ribonucleic acid 29, highly up-regulated in diabetic rats, leads to insulin resistance in 3T3-L1 adipocytes. Mol. Endocrinol. 21, 2785–2794. https://doi.org/10.1210/me.2007-0167.

Hiroki, E., Akahira, J., Suzuki, F., Nagase, S., Ito, K., Suzuki, T., Sasano, H., and Yaegashi, N. (2010). Changes in microRNA expression levels correlate with clinicopathological features and prognoses in endometrial serous adenocarcinomas. Cancer Sci. 101, 241–249. https://doi.org/10.1111/j.1349-7006.2009.01385.x.

Horita, M., Farquharson, C., and Stephen, L.A. (2021). The role of miR-29 family in disease. J. Cell Biochem. 122, 696–715. https://doi.org/10.1002/jcb.29896.

Huang, J., Yin, H., Rao, S.S., Xie, P.L., Cao, X., Rao, T., Liu, S.Y., Wang, Z.X., Cao, J., Hu, Y., et al. (2018). Harmine enhances type H vessel formation and prevents bone loss in ovariectomized mice. Theranostics 8, 2435–2446. https://doi.org/10.7150/thno.22144.

Ikebuchi, Y., Aoki, S., Honma, M., Hayashi, M., Sugamori, Y., Khan, M., Kariya, Y., Kato, G., Tabata, Y., Penninger, J.M., et al. (2018). Coupling of bone resorption and formation by RANKL reverse signalling. Nature 561, 195–200. https://doi.org/10.1038/s41586-018-0482-7.

Johnson, R.W., Schipani, E., and Giaccia, A.J. (2015). HIF targets in bone remodeling and metastatic disease. Pharmacol. Ther. 150, 169–177. https://doi.org/10.1016/j.pharmthera.2015.02.002.

Jones, D.C., Wein, M.N., Oukka, M., Hofstaetter, J.G., Glimcher, M.J., and Glimcher, L.H. (2006). Regulation of adult bone mass by the zinc finger adapter protein Schnurri-3. Science 312, 1223–1227. https://doi.org/10.1126/science.1126313.

Joshi, G.K., Deitz-Mcelyea, S., Liyanage, T., Lawrence, K., Mali, S., Sardar, R., and Korc, M. (2015). Label-free nanoplasmonic-based short noncoding RNA sensing at attomolar concentrations allows for quantitative and highly specific assay of MicroRNA-10b in biological fluids and circulating exosomes. ACS Nano 9, 11075–11089. https://doi.org/10.1021/acsnano.5b04527.

Kaelin, W.G., Jr., and Ratcliffe, P.J. (2008). Oxygen sensing by metazoans: The central role of the HIF hydroxylase pathway. Mol. Cell 30, 393–402. https://doi.org/10.1016/j.molcel.2008.04.009.

Kenkre, J.S., and Bassett, J. (2018). The bone remodelling cycle. Ann. Clin. Biochem. 55, 308–327. https://doi.org/10.1177/0004563218759371.

Kloosterman, W.P., and Plasterk, R.H. (2006). The diverse functions of microRNAs in animal development and disease. Dev. Cell 11, 441–450. https://doi.org/10.1016/j.devcel.2006.09.009.

Ko, J.Y., Chuang, P.C., Ke, H.J., Chen, Y.S., Sun, Y.C., and Wang, F.S. (2015). MicroRNA-29a mitigates glucocorticoid induction of bone loss and fatty marrow by rescuing Runx2 acetylation. Bone 81, 80–88. https://doi.org/10.1016/j.bone.2015.06.022.

Kodahl, A.R., Lyng, M.B., Binder, H., Cold, S., Gravgaard, K., Knoop, A.S., and Ditzel, H.J. (2014). Novel circulating microRNA signature as a potential non-invasive multi-marker test in ER-positive early-stage breast cancer: a case control study. Mol. Oncol. 8, 874–883. https://doi.org/10.1016/j.molonc.2014.03.002.

Kriegel, A.J., Liu, Y., Fang, Y., Ding, X., and Liang, M. (2012). The miR-29 family: genomics, cell biology, and relevance to renal and cardiovascular injury. Physiol. Genomics 44, 237–244. https://doi.org/10.1152/physiolgenomics.00141.2011.

Krzeszinski, J.Y., Wei, W., Huynh, H., Jin, Z., Wang, X., Chang, T.C., Xie, X.J., He, L., Mangala, L.S., Lopez-Berestein, G., et al. (2014). miR-34a blocks osteoporosis and bone metastasis by inhibiting osteoclastogenesis and Tgif2. Nature 512, 431–435. https://doi.org/10.1038/nature13375.

Kusumbe, A.P., Ramasamy, S.K., and Adams, R.H. (2014). Coupling of angiogenesis and osteogenesis by a specific vessel subtype in bone. Nature 507, 323–328. https://doi.org/10.1038/nature13145.

Li, C.-J., Cheng, P., Liang, M.-K., Chen, Y.-S., Lu, Q., Wang, J.-Y., Xia, Z.-Y., Zhou, H.-D., Cao, X., Xie, H., et al. (2015). MicroRNA-188 regulates age-related switch between osteoblast and adipocyte differentiation. J. Clin. Invest. 125, 1509–1522. https://doi.org/10.1172/jci77716.

Liao, Y., Ouyang, L., Ci, L., Chen, B., Lv, D., Li, Q., Sun, Y., Fei, J., Bao, S., Liu, X., et al. (2019). Pravastatin regulates host foreign-body reaction to polyetheretherketone implants via miR-29ab1-mediated SLIT3 upregulation. Biomaterials 203, 12–22. https://doi.org/10.1016/j.biomaterials.2019.02.027.

Liu, Y., Taylor, N.E., Lu, L., Usa, K., Cowley, A.W., Jr., Ferreri, N.R., Yeo, N.C., and Liang, M. (2010). Renal medullary microRNAs in Dahl salt-sensitive rats: miR-29b regulates several collagens and related genes. Hypertension 55, 974–982. https://doi.org/10.1161/hypertensionaha.109.144428.

Ma, J., Lin, X., Chen, C., Li, S., Zhang, S., Chen, Z., Li, D., Zhao, F., Yang, C., Yin, C., et al. (2020). Circulating miR-181c-5p and miR-497-5p are potential biomarkers for prognosis and diagnosis of osteoporosis. J. Clin. Endocrinol. Metab. 105. https://doi.org/10.1210/clinem/dgz300.

Maes, C., Kobayashi, T., Selig, M.K., Torrekens, S., Roth, S.I., Mackem, S., Carmeliet, G., and Kronenberg, H.M. (2010). Osteoblast precursors, but not mature osteoblasts, move into developing and fractured bones along with invading blood vessels. Dev. Cell 19, 329–344. https://doi.org/10.1016/j.devcel.2010.07.010.

Maynard, M.A., Evans, A.J., Hosomi, T., Hara, S., Jewett, M.A., and Ohh, M. (2005). Human HIF-3alpha4 is a dominant-negative regulator of HIF-1 and is down-regulated in renal cell carcinoma. FASEB J. 19, 1396–1406. https://doi.org/10.1096/fj.05-3788com.

Nakashima, K., Zhou, X., Kunkel, G., Zhang, Z., Deng, J.M., Behringer, R.R., and De Crombrugghe, B. (2002). The novel zinc finger-containing transcription factor Osterix is required for osteoblast differentiation and bone formation. Cell 108, 17–29. https://doi.org/10.1016/s0092-8674(01)00622-5.

Noren Hooten, N., Abdelmohsen, K., Gorospe, M., Ejiogu, N., Zonderman, A.B., and Evans, M.K. (2010). microRNA expression patterns reveal differential expression of target genes with age. PLoS One 5, e10724. https://doi.org/10.1371/journal.pone.0010724.

Pan, T., Song, W., Gao, H., Li, T., Cao, X., Zhong, S., and Wang, Y. (2016). miR-29b-loaded gold nanoparticles targeting to the endoplasmic reticulum for synergistic promotion of osteogenic differentiation. ACS Appl. Mater. Inter. 8, 19217–19227. https://doi.org/10.1021/acsami.6b02969.

Peng, Y., Wu, S., Li, Y., and Crane, J.L. (2020). Type H blood vessels in bone modeling and remodeling. Theranostics 10, 426–436. https://doi.org/10.7150/thno.34126.

Ramasamy, S.K., Kusumbe, A.P., Schiller, M., Zeuschner, D., Bixel, M.G., Milia, C., Gamrekelashvili, J., Limbourg, A., Medvinsky, A., Santoro, M.M., et al. (2016). Blood flow controls bone vascular function and osteogenesis. Nat.

Commun. 7, 13601. https://doi.org/10.1038/ncomms13601.

Ramasamy, S.K., Kusumbe, A.P., Wang, L., and Adams, R.H. (2014). Endothelial Notch activity promotes angiogenesis and osteogenesis in bone. Nature 507, 376–380. https://doi.org/10.1038/nature13146.

Saito, T., Fukai, A., Mabuchi, A., Ikeda, T., Yano, F., Ohba, S., Nishida, N., Akune, T., Yoshimura, N., Nakagawa, T., et al. (2010). Transcriptional regulation of endochondral ossification by HIF-2alpha during skeletal growth and osteoarthritis development. Nat. Med. 16, 678–686. https://doi.org/10.1038/nm.2146.

Schwarzenbach, H., Nishida, N., Calin, G.A., and Pantel, K. (2014). Clinical relevance of circulating cell-free microRNAs in cancer. Nat. Rev. Clin. Oncol. 11, 145–156. https://doi.org/10.1038/nrclinonc.2014.5.

Small, E.M., Sutherland, L.B., Rajagopalan, K.N., Wang, S., and Olson, E.N. (2010). MicroRNA-218 regulates vascular patterning by modulation of Slit-Robo signaling. Circ. Res. 107, 1336–1344. https://doi.org/10.1161/CIRCRESAHA.110.227926.

Sun, J., Feng, H., Xing, W., Han, Y., Suo, J., Yallowitz, A.R., Qian, N., Shi, Y., Greenblatt, M.B., and Zou, W. (2020). Histone demethylase LSD1 is critical for endochondral ossification during bone fracture healing. Sci. Adv. 6. https://doi.org/10.1126/sciadv.aaz1410.

Vanderwalde, A., and Hurria, A. (2011). Aging and osteoporosis in breast and prostate cancer. CA Cancer J. Clin. 61, 139–156. https://doi.org/10.3322/caac.20103.

Wang, H., Deng, Q., Lv, Z., Ling, Y., Hou, X., Chen, Z., Dinglin, X., Ma, S., Li, D., Wu, Y., et al. (2019). N6-methyladenosine induced miR-143-3p promotes the brain metastasis of lung cancer via regulation of VASH1. Mol. Cancer 18, 181. https://doi.org/10.1186/s12943-019-1108-x.

Wang, L., Zhou, F., Zhang, P., Wang, H., Qu, Z., Jia, P., Yao, Z., Shen, G., Li, G., Zhao, G., et al. (2017). Human type H vessels are a sensitive biomarker of bone mass. Cell Death Dis. 8, e2760. https://doi.org/10.1038/cddis.2017.36.

Widlansky, M.E., Jensen, D.M., Wang, J., Liu, Y., Geurts, A.M., Kriegel, A.J., Liu, P., Ying, R., Zhang, G., Casati, M., et al. (2018). miR-29 contributes to normal endothelial function and can restore it in cardiometabolic disorders. EMBO Mol. Med. 10, e8046. https://doi.org/10.15252/emmm.201708046.

Xie, H., Cui, Z., Wang, L., Xia, Z., Hu, Y., Xian, L., Li, C., Xie, L., Crane, J., Wan, M., et al. (2014). PDGF-BB secreted by preosteoclasts induces angiogenesis during coupling with osteogenesis. Nat. Med. 20, 1270–1278. https://doi.org/10.1038/nm.3668.

Xu, R., Yallowitz, A., Qin, A., Wu, Z., Shin, D.Y., Kim, J.M., Debnath, S., Ji, G., Bostrom, M.P., Yang, X., et al. (2018). Targeting skeletal endothelium to ameliorate bone loss. Nat. Med. 24, 823–833. https://doi.org/10.1038/s41591-018-0020-z.

Xuan, Y., Sun, L.H., Liu, D.M., Zhao, L., Tao, B., Wang, W.Q., Zhao, H.Y., Liu, J.M., and Ning, G. (2015). Positive association between serum levels of bone resorption marker CTX and HbA1c in women with normal glucose tolerance. J. Clin. Endocrinol. Metab. 100, 274–281. https://doi.org/10.1210/jc.2014-2583.

Yang, M., Li, C.J., Sun, X., Guo, Q., Xiao, Y., Su, T., Tu, M.L., Peng, H., Lu, Q., Liu, Q., et al. (2017). MiR-497 approximately 195 cluster regulates angiogenesis during coupling with osteogenesis by maintaining endothelial Notch and HIF-1alpha activity. Nat. Commun. 8, 16003. https://doi.org/10.1038/ncomms16003.

Yang, S.L., Wu, C., Xiong, Z.F., and Fang, X. (2015). Progress on hypoxia-inducible factor-3: its structure, gene regulation and biological function (Review). Mol. Med. Rep. 12, 2411–2416. https://doi.org/10.3892/mmr.2015.3689.

Zaidi, M. (2007). Skeletal remodeling in health and disease. Nat. Med. 13, 791–801. https://doi.org/10.1038/nm1593.

Zeng, Q., Wang, Y., Gao, J., Yan, Z., Li, Z., Zou, X., Li, Y., Wang, J., and Guo, Y. (2019). miR-29b-3p regulated osteoblast differentiation via regulating IGF-1 secretion of mechanically stimulated osteocytes. Cell Mol. Biol. Lett. 24, 11. https://doi.org/10.1186/s11658-019-0136-2.

Zhang, J.F., Fu, W.M., He, M.L., Wang, H., Wang, W.M., Yu, S.C., Bian, X.W., Zhou, J., Lin, M.C., Lu, G., et al. (2011). MiR-637 maintains the balance between adipocytes and osteoblasts by directly targeting Osterix. Mol. Biol. Cell 22, 3955–3961. https://doi.org/10.1091/mbc.E11-04-0356.

Zhang, P., Yao, Q., Lu, L., Li, Y., Chen, P.J., and Duan, C. (2014). Hypoxia-inducible factor 3 is an oxygen-dependent transcription activator and regulates a distinct transcriptional response to hypoxia. Cell Rep. 6, 1110–1121. https://doi.org/10.1016/j.celrep.2014.02.011.

STAR★METHODS

KEY RESOURCES TABLE

REAGENT or RESOURCE	SOURCE	IDENTIFIER
Antibodies		
Mouse monoclonal CD31 antibody	Abcam	Cat# ab24590; RRID: AB_448167
Mouse monoclonal EMCN antibody	Santa Cruz	Cat# sc-65495; RRID: AB_2100037
Rabbit polyclonal Runx-2 antibody	Abcam	Cat# ab23981; RRID: AB_777785
Rabbit monoclonal Anti- p7/Osterix antibody	Abcam	Cat# ab209484; RRID: AB_2892207
Rabbit monoclonal HIF-1β antibody	Abcam	Cat# ab239366
Rabbit polyclonal HIF-3α antibody	Novus	Cat# NB100-2287SS; RRID: AB_790150
Mouse monoclonal HIF-1β antibody	Abcam	Cat# ab2771; RRID: AB_303284
Rabbit polyclonal HIF-3α antibody	Novus	Cat# NBP1-03155; RRID: AB_2117409
Critical commercial assays		
OCN	Rochediagnostics	Cat#11972111 122
PTH	Rochediagnostics	Cat#07251068 190
CTx	Rochediagnostics	Cat#11972308 122
25OHVitD	Rochediagnostics	Cat#05894913 190
Deposited data		
RNA sequence	NCBI	GSE188697
Experimental models: Organisms/strains		
Homozygous miR-29cb2$^{-/-}$ mice (C57BL/6J strain)	Shanghai Model Organisms Center	N/A
Software and algorithms		
Image J	N/A	N/A

RESOURCE AVAILABILITY

Lead contact

Further information and requests for resources and reagents should be directed to and will be fulfilled by the lead contact, Dr. Yun Liao (libra_ly@shsmu.edu.cn).

Materials availability

- Knockout mice used in this study were generated by Shanghai Model Organisms Center (Shanghai, China)

- This study did not generate any new reagents

Data and code availability

- All data needed to evaluate the conclusions in the paper are present in the paper and/or the supplemental information. Any additional information required to reanalyze the data reported in this paper is available from the lead contact upon request.

- All data reported in this paper will be shared by the lead contact upon request

- This paper does not report original code.

EXPERIMENTAL MODEL AND SUBJECT DETAILS

All animals were housed in specific pathogen-free environment with a 12 h light/dark cycle with food and water ad libitum. This study was performed in strict accordance with institutional guidelines and the animal

institutional licence is SCXK (HU) 2019-0002. This study approved by the Institutional Animal Care and Use Committee in Shanghai Model Organisms Center and Shanghai Tenth People's Hospital, the IACUC permit numbers were 2019-0002 and SHDSYY-2015-0018 respectively. All human experiments were carried out with approval from the Shanghai Tongren Hospital Ethics Committee (no. 2020-025-01).

Homozygous miR-29cb2$^{-/-}$ mice (C57BL/6J strain) were generated using the CRISPR/Cas9 technique. miR-29cb2$^{-/-}$ mice were generated as follows: guide RNAs (gRNAs) were designed to target the 5′ and 3′ ends of mouse miR-29c/b2 based on publicly available information on the sequences of miR-29c (MGI 3619047, http://www.informatics.jax.org/marker/MGI:3619047) and miR-29b2 (MGI 2676906, http://www.informatics.jax.org/marker/MGI:2676906). The spacer sequences of the gRNAs were as follows: gRNA1, 5′-GGCTGTCATCTGCGTCTGACAGG-3′; gRNA2, 5′-ATGATTCTCAGGGCTGAGGCTGG-3′; gRNA3, 5′-GCACCAGCCTCAGAACCTT GTGG-3′; and gRNA4, 5′-TCAGCCTATCACTTCCTACGTGG-3′. Homozygous mice were bred for at least four generations at the Shanghai Model Organisms Center (Shanghai, China) before any experiments were begun (Figure S14). Six weeks and sixteen weeks female miR-29cb2$^{-/-}$ mice were used for further studies (IACUC number 2019-0002).

Female mice (C57BL/6J, n = 18; 8 weeks old, 20 ± 2.5 g) were obtained from the Shanghai Model Organisms Center, China. Surgery was performed as follows: First, mice were anesthetized by intraperitoneal injection of isoflurane gas. Then, a single small dorsal incision was made in each side, and the subcutaneous connective tissue was separated to expose the ovary. The ovary was removed by severing the oviduct. Then, the wound was carefully closed, and mice were fed ad libitum for 8 weeks. All animal care protocols complied with the Laboratory Animal Care and Use Guidelines of Shanghai Tenth People's Hospital (IACUC number SHDSYY-2015-0018).

Forty-five to eighty years old patients of arbitrary sex were randomly selected for biomarkers determination. Nine females and six males were included into osteopenia group. Seven females were included into osteoporosis group. Age statistics of patients are shown in Figure S11. Sixty-one to seventy-nine years old patients (4 females and 2 males) who required knee replacement surgery were selected for bone samples collection. The fresh samples obtained were divided in several parts for PCR, western blotting and immunostaining analysis. Informed consent was obtained from all patients, and this process was approved by the Institutional Review Board of Tongren Hospital, Shanghai Jiao Tong University School of Medicine (no. 2020-025-01).

METHOD DETAILS
Labeling of CD31^{hi}EMCN^{hi} vessels

miR-29cb2$^{-/-}$ mice were sacrificed at the ages of 6 and 16 weeks. The femurs were collected and fixed with 4% paraformaldehyde (PFA) for more than 1 day. Then, the samples were carefully transferred into decalcifying solution, which was refreshed daily. After one month, the femurs were dehydrated overnight in a tissue processor and embedded in paraffin. anti-CD31 (mouse, 1:100, ab24590, Abcam) and monoclonal anti-EMCN (rat, 1:100, sc-65495, Santa Cruz) antibodies were used to label CD31 and EMCN, whose high expression is a marker of neovascularization. Immunohistochemical images were acquired by fluorescence microscopy (Olympus, IX-71) with a digital Olympus camera. Digital images showing each antigen were acquired and evaluated using Image-Pro Plus software.

BONE ANALYSIS
Micro-CT evaluation

miR-29cb2$^{-/-}$ mice were sacrificed at the ages of 6 and 16 weeks. The femurs were collected and fixed with 4% PFA for more than 1 day. A micro-CT system (Skyscan 1172, Bruker Micro-CT, Germany) was used to identify the bone mass. Scanning was performed using an Al 1-mm filter at 65 kV with a resolution of 18 mm. Two-dimensional (2D) and three-dimensional (3D) images were reconstructed with NRecon software and the CTvol program.

Histopathological evaluation

miR-29cb2$^{-/-}$ mice were sacrificed at the ages of 6 and 16 weeks. The femurs were collected, fixed with 4% PFA, decalcified and cut into 6 μm thick transverse sections. HE (Servicebio), an anti-Runx-2 antibody (rabbit; 1:1000; ab23981; Abcam), Anti-Sp7 / Osterix antibody (Rabbit; 1:1000; ab209484; Abcam) and

Trap (Servicebio) were used for morphological examination. anti-HIF-1β (rabbit; 1:1000; ab2771; Abcam) and anti-HIF-3α (rabbit; 1:14000; NBP1-03155; Novus) were used for target examination. Digital images showing each antigen were acquired and evaluated using Image-Pro Plus software.

RNA-seq and analysis

Reads were aligned to the mm10 mouse transcripts using STAR (1.2.0) with the default parameters. The DESeq2 R (1.16.1) R package was used to normalize gene count data and then detect DEGs (false discovery rate < 0.1 and absolute log2 (fold change) > 0.5) between miR-29cb2$^{-/-}$ mice and control mice.

Luciferase activity

Fluorescein-labeled reporter gene detection was carried out using a Dual Luciferase Assay System kit (Promega) after sequence comparisons of *hif-3α* and miRNAs, according to the manufacturer's instructions. Wild-type and two mutant pmiRGlo-*hif-3α*-3′UTR dual luciferase reporter vectors incorporating miRNA binding sites were constructed. HEK293 cells were co-transfected with wild-type or mutant vectors and miRNA mimics using transfection reagents for 48 h. The cells were lysed to detect the luciferase activities using the Luciferase Reporter Assay Kit.

Quantitative RT-PCR (qRT-PCR)

Femurs of WT and miR-29cb2$^{-/-}$ mice were collected and immediately stored in liquid nitrogen. Gene expression was analyzed by qRT-PCR (LightCycler 480 Real-Time PCR System, Roche, Basel, Switzerland). The primer sequences are listed in Table S4. qRT-PCR experiments were performed with at least two independent replicates, and each sample was analyzed in duplicate. Relative expression was quantified using the comparative threshold method. Data are expressed as $2^{-\Delta\Delta Ct}$ values.

Western blotting analysis

Western blotting analysis was performed to assess protein expression. Femur samples were homogenized, and protein was extracted via incubation in RIPA lysis buffer (bioTNT) and centrifugation. Then, 20 μg of protein from each sample was separated via SDS-PAGE and transferred to nitrocellulose membranes. TBS-Tween 20 buffer with 5% BSA was added to block the membranes for 1 h, and the membranes were then incubated with anti-HIF-1β (rabbit; 1:1000; ab239366; Abcam) and anti-HIF-3α (rabbit; 1:200; NB100-2287SS; Novus) primary antibodies overnight at 4°C. Horseradish peroxidase-conjugated secondary antibodies were then added and incubated with the membranes for 1 h at room temperature. Protein bands were visualized using alphaEaseFC (Alpha Innotech, USA) in a darkroom.

HUMAN SAMPLE COLLECTION AND ASSESSMENT

Human distal femur evaluation

Patients obtained X-ray san score range from −1 to −2.5 were into the osteopenia group and greater than −2.5 were into osteoporosis group (Camacho et al., 2020). Patients with osteoporosis or osteopenia who underwent knee replacement surgery were included. Patients with the following comorbidities or conditions were excluded: microbial infection in the knee; bone tumors; systemic bone-related metabolic endocrine diseases; and treatment with hormones, steroids, vitamin D or calcium.

Peripheral blood (PB) collection and miR-29cb2 detection

PB (2 mL) remaining from preoperative routine blood tests of the patients who underwent joint-related surgery were included. To prevent RNA degradation, whole blood was collected into PAXgene Blood RNA tubes for subsequent detection. Then, total RNA was concentrated and purified using a PAXgene Blood RNA kit. In brief, the pellet collected from the initial centrifugation was incubated in optimized buffers with proteinase K to digest proteins. After incubation at 55°C for 10 min, the suspension was transferred to a PAXgene Shredder spin column (PSC) to homogenize the cell lysate and remove residual cell debris. After adding ethanol to the aforementioned supernatant to adjust the binding conditions, the lysate was applied to a PAXgene RNA spin column (PRC). During a brief centrifugation step, the RNA was selectively bound to the silica membrane of the PAXgene column as contaminants passed through. The remaining contaminants were removed through several efficient wash steps. Between the first and second wash steps, the membrane was treated with DNase I (RNFD) to remove trace amounts of bound DNA. After the wash steps, RNA was eluted in elution buffer and heat denatured, it was then ready for subsequent detection. miR-29 family members were detected by RT-PCR as described above.

Biomarkers evaluation

Four types of biomarkers were evaluated according to the product manual: OCN (Rochediagnostics 11972111 122), PTH (Rochediagnostics, 07251068 190), CTx (Rochediagnostics, 11972308 122) and 25OHVitD (Rochediagnostics, 05894913 190).

QUANTIFICATION AND STATISTICAL ANALYSIS

All data are expressed as the means $\pm$ standard errors and were analyzed using GraphPad Prism Version 5.0 statistical software (GraphPad Software, CA, USA). One-way ANOVA and Student's t-test with the Bonferroni post hoc test were used for comparisons among groups and within each group, respectively. ROC analysis was performed to calculate the AUC values along with the standard errors and 95% confidence intervals. Statistical significance was accepted at $p < 0.05$.